

Integration of Leaky and Surface Waves in a 2D Gaussian Beam Formalism for Antenna-Structure Coupling

Olivier Balosso^{1, 2, 3, *}, Jerome Sokoloff³, and Sylvain Bolioli¹

Abstract—Gaussian beam techniques are efficient asymptotic methods for field radiation computation. In these techniques, the initial field is first expanded on a chosen surface in elementary Gaussian beams which can propagate and/or interact with surrounding structures. However, the expansion cannot take into account surface and leaky waves propagation. In this paper, we propose an appropriate hybridization method using surface equivalent currents to overcome this limitation. The equivalent current formulation is written on grounded dielectric slab in spectral domain and can model surface and leaky waves which propagate from the surface expansion. The hybridization is carried out on the expansion surface, on which the distribution of elementary Gaussian beams and equivalent currents must be chosen in a relevant way. We study the influence of hybridization parameters and define a set of them leading to good results for general cases.

1. INTRODUCTION

High-frequency techniques are successfully applied to describe electromagnetic wave radiation. However, as objects under consideration become large compared to the wavelength, rigorous approaches such as the finite-element method or the method of moments become computer time and resource prohibitive. By contrast, the efficiency of asymptotic methods such as geometrical optics and physical optics increases with frequency. However they become ill-suited for complex cases because of the increasing number of iterations. In these cases Gaussian Beam (GB) techniques could be efficient alternatives [1–10]. During the last decade our team has worked on these techniques leading to original GB expansion [7, 8], closed form expressions for GB reflection/refraction by curved multilayer dielectrics such as radomes [7, 8], diffraction by metallic plate [9] or, more recently, GB interaction with dichroic surfaces [10]. However, with our current GB decomposition method, we cannot close the decomposition domain near the interface which holds the antenna. In this area, the field strongly interacts with the interface and hence could excite Surface Waves (SW) and Leaky Waves (LW). Our GB method cannot model these types of phenomena. Besides, in the context of microwave device miniaturization as well as the study of the antenna-structure coupling, it becomes essential to model SW and LW excitation, as they take part in coupling phenomena [11, 12]. Furthermore, the excitation of SW and LW by elementary current line sources has been studied extensively [13–15] using the surface equivalent current theorem [16]. Therefore, in this paper, we propose a method to hybridize the GB expansion and the surface equivalent current expansion in order to model the excitation of SW and LW on a Grounded Dielectric Slab (GDS).

This paper is organized as follows. In Section 2, after a short presentation of the main existing formulations leading to GB, we present the GB method and illustrate its use on a complex electromagnetic problem. In Section 3, we study the Transverse Magnetic (TM) excitation of a GDS by magnetic and electric current sources by extending the theory presented in [13, 14]. Then, we present

Received 30 January 2014, Accepted 24 February 2014, Scheduled 4 March 2014

* Corresponding author: Olivier Balosso (olivier.balosso.pro@gmail.com).

¹ Onera — The French Aerospace Lab, 2 av. Edouard Belin, Toulouse F-31055, France. ² CNES, Service Antennes, 18 av. Edouard Belin, Toulouse F-31401, France. ³ UPS, INPT; LAPLACE (Laboratoire Plasma et Conversion d’Energie), Université de Toulouse, 118 Route de Narbonne, Toulouse Cedex 9 F-31062, France.

in Section 4 the hybridization method we developed in order to extend the GB expansion to take into account SW and LW on GDS. We present the method principle with its performances and define a default parameter setting able to treat general cases. Finally, in Section 5, we discuss in which extent finer settings can lead to further improved results.

An $\exp(+j\omega t)$ time dependence for electromagnetic fields is assumed and suppressed throughout this paper. All this work is carried out in 2D (in the xOz plane) and all fields used are TM polarized. However the transposition of this study to Transverse Electric (TE) cases is trivial [14]. Structures studied here are GDS only; however the hybridization principle is the same for dielectric slabs or multilayer structures [14, 17, 18].

2. GAUSSIAN BEAM METHOD

In this part, we present the GB method we use. We start by a short presentation of existing formulations leading to GB. Then we describe the GB expansion method used. Finally we illustrate how we use this method to solve a complex electromagnetic problem.

2.1. Gaussian Beam

A Gaussian Beam (GB) is a beam of electromagnetic radiation which transverse electromagnetic field distribution is well approximated by gaussian functions. It was first defined for laser sources in optics using the paraxial approximation [19]. This approximation allows to obtain a closed form expression on the GB, but requires that the field is only weakly divergent (i.e., less than 20°) along its main propagation direction. Moreover, in the far field region, the paraxial approximation produces an important phase error [1, 7]. To overcome these limitations, other expressions were found to define the GB. When representing the GB's field at its waist in terms of angular plane wave spectrum and then propagating this spectrum, another closed form expression is found using the far field approximation [7]. The GB can also be defined as a complex source point [1]. This latter expression results exactly from Maxwell's equations and thus does not require any approximation; however it can only describe circular GB. Lately our team has developed a GB, called "conformal GB" [8]. It is defined by the currents at its waist, allowing this GB to be launched by highly curved surfaces.

Figure 1 shows the field amplitude of a 2D GB propagating along the z axis. W_0 is the GB's waist (width at $z = 0$) and θ_x , defines the divergence angle as follows:

$$\theta_x = \frac{2}{k \cdot W_0} \quad (1)$$

with k the wave number in the propagating medium. The field amplitude at $x = W_0$ is 8.7 dB under the amplitude at $x = 0$. We define the parameter α which allows us to describe the so-called useful width of the GB. This parameter will be used in Section 4.

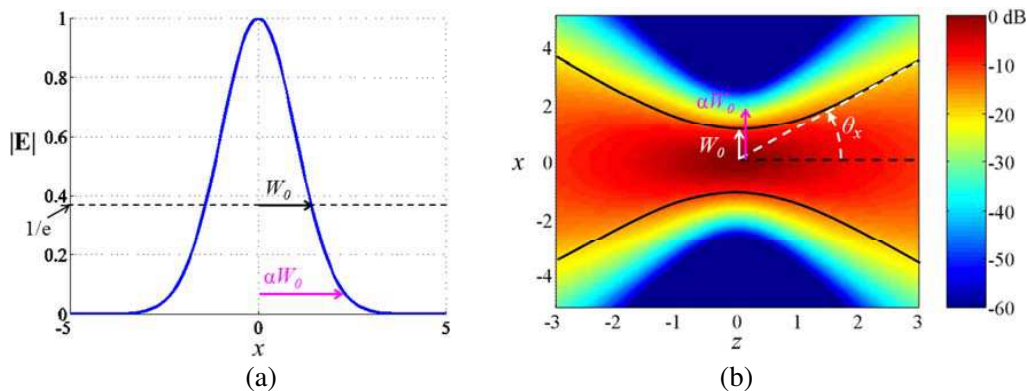


Figure 1. Field amplitude of a GB propagating along the z axis: (a) transverse cut in its waist plane ($z = 0$); (b) longitudinal cut in the xOz plane, in dB.

Besides, closed form expressions exist for the interaction of paraxial GBs with complex structures [7–10]. Thus, in this article, all GBs used are purposely chosen in order to respect the paraxial approximation ($\theta_x < 20^\circ$). However, as the aim of this paper is to study the accuracy of our hybridization technique, we use complex source point GBs in order to obtain results free from any error linked to paraxial approximation.

2.2. Gaussian Beam Expansion

An electromagnetic field can be expressed in terms of a set of GBs shifted both in position and in propagation direction [7]. Figure 2 illustrates this decomposition for a TM field. We assume that the initial field \mathbf{H}^i on the expansion surface is known and regular. Moreover, the size and the curvature radius of the expansion surface must be large compared to the wavelength. Each elementary beam has its own reference (O_n, \mathbf{e}_{zn}) , where O_n stands for the n th-beam center and \mathbf{e}_{zn} for the n th-beam propagation axis. The characteristics of each elementary beam have to be determined. The beam centers O_n are regularly distributed on the expansion surface from a mesh of step d_{GB} . Contrary to the Gabor expansion, only one beam is defined on each beam center. In order to suit the local properties of the electromagnetic fields well, each elementary beam propagation axis is oriented along the local Poynting vector ($\mathbf{e}_{zn} = \mathbf{P}_n/|\mathbf{P}_n|$).

The expansion coefficients are computed by a point matching technique: on the mesh points, we project the equality between the initial magnetic field and the beam expansion. The solution of this linear system gives the GB coefficients.

The characteristics of the elementary beam set only depend on the choice of two related parameters: the waist W_0 and the mesh step d_{GB} . It has been shown in [7] that a good compromise between accuracy and computation time can be obtained with d_{GB} varying between λ and 2λ and $W_0 = d_{GB}/0.9$.

2.3. Gaussian Beam Method Applied to a Complex Electromagnetic Problem

GBs expansion, propagation, interaction and recombination are jointly used to solve complex electromagnetic problems [7–10]. Figure 3 presents an antenna placed on a Grounded Dielectric Slab (GDS) of thickness d and surrounded by air. It radiates an electromagnetic field in a complex environment. In order to solve the total field with the GB method we proceed as follows: the radiated field is expanded on surface S_{exp} in terms of a few elementary GBs (red lines), each one of them propagates through free space (grey arrows) until it meets an object. Then we solve analytically the reflected, transmitted or diffracted field, depending on the object met [7–10]. When the object is met under moderate incidence angle and presents a smooth and regular surface, we can assume that an incident GB gives a reflected GB and a transmitted GB which can, in their turn, propagate and interact. Otherwise, reflected and transmitted fields are analytically computed on the object’s interface and expanded again in GB. When all interactions are treated, the total resulting field is obtained by combining the fields of all final GBs. However a non null field near the interface cannot be expanded in terms of GBs. To close the decomposition domain, the GB expansion must be hybridized with an

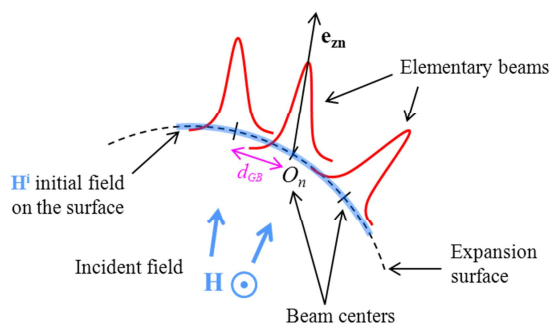


Figure 2. Beam expansion principle.

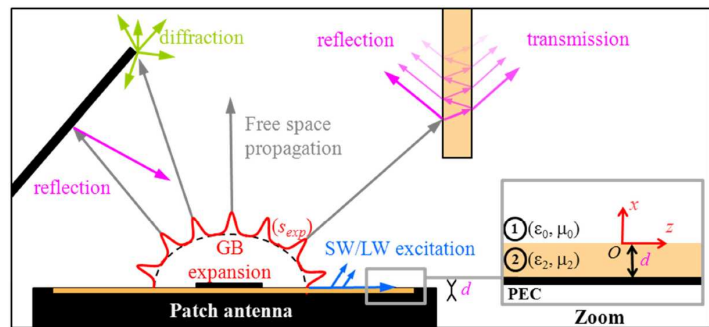


Figure 3. Operating principle for electromagnetic computation using GB field expansion.

appropriate method. In this paper, we chose to use the Surface Equivalent Current (SEC) technique [16] to do so.

3. COMPLEX WAVE EXCITATION ON A GROUNDED DIELECTRIC SLAB BY A CURRENT LINE SOURCE

We aim at expanding the 2D TM electromagnetic field close to the interface in the media 1 and 2 in terms of Surface Equivalent Currents (SEC). The configuration, which can be seen in the zoom area in Figure 3, is depicted in detail on Figure 4. In this area, the total field is a combination of, on the one hand, the field directly radiated by the currents and, on the other hand, its interactions with the Grounded Dielectric Slab (GDS) in terms of reflected field, Surface Wave and Leaky Wave. Thus, in this part, we study excitation of a GDS structure by magnetic and electric elementary currents respectively.

Figure 4 presents a 2D GDS infinite along \mathbf{e}_z and invariant along the y direction. This structure is excited by an elementary current line source s placed at $z = 0$ and $x = x_s$. We are willing to compute the magnetic field \mathbf{H} at any point M located in medium 1 or 2.

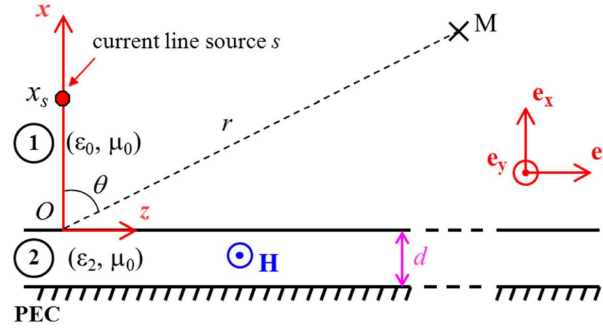


Figure 4. Excitation of a grounded dielectric slab by a current line source. Medium 1 is air, medium 2 is a dielectric (ε_2) and the slab thickness is d .

3.1. Ground Dielectric Slab's Excitation by a Magnetic Current Source

In this part, the source s in Figure 4 is a magnetic current line source oriented along \mathbf{e}_y . The field can therefore only be TM with the magnetic field \mathbf{H} oriented along \mathbf{e}_y . This case has been studied extensively by Tamir in [13,14] and Collins in [15]. \mathbf{H} is derived from the Helmholtz equation in presence of a magnetic source \mathbf{M} located at $z = 0$ and $x = x_s$.

$$(\nabla^2 + k^2) \mathbf{H}(x, z) = j \cdot \omega \varepsilon \cdot \mathbf{M} \delta(x - x_s) \delta(z) \quad (2)$$

with k and ε the wave number and the permittivity, respectively, in the considered medium; j defined by $j^2 = -1$ and δ denoting the Dirac delta function.

The spectral representation of \mathbf{H} is calculated by applying the boundary conditions at $x = -d$, $x = 0$, $x = x_s$ and $x \rightarrow \infty$. The spectral integration takes place on the real k_z axis, with k_z the z component of the wave vector \mathbf{k} . The initial integration contour is then deformed in the Steepest Decent Path (SDP). A pole p of the spectral reflection or transmission coefficient may be captured during the spectral integration along the SDP, giving rise to a residue contribution \mathbf{H}_p . The total field is then given by $\mathbf{H} = \mathbf{H}_S + \Sigma \mathbf{H}_p$, with \mathbf{H}_S resulting from the spectral integration along the SDP and $\Sigma \mathbf{H}_p$ being the contribution of the captured poles. The spectral integration is achieved numerically or analytically, respectively, depending on whether M is near or far ($k_1 \cdot r \gg 1$, [13]) from the source s . Resulting expressions for \mathbf{H}_S and \mathbf{H}_p can be found in [14].

3.2. Ground Dielectric Slab's Excitation by an Electric Current Source

In order to excite a TM field with an electric current line source, the associated current \mathbf{J} must belong to the xOz plan. The Helmholtz equation then writes:

$$(\nabla^2 + k^2) \mathbf{H}(x, z) = -\nabla \times \mathbf{J} \delta(x - x_s) \delta(z) \quad (3)$$

When writing (3) in terms of plane wave angular spectrum, we obtain Equation (4) representing the problem's source dependency.

$$\left. \frac{\partial \hat{\mathbf{H}}}{\partial x} \right|_{x=x_{S+}} = \left. \frac{\partial \hat{\mathbf{H}}}{\partial x} \right|_{x=x_{S-}} + j \cdot (k_z J_x - k_x J_z) \cdot \mathbf{e}_y \quad (\text{at } x = x_S) \quad (4)$$

$\hat{\mathbf{H}}$ being the Fourier transform of \mathbf{H} and J_x and J_z being respectively x and z components of \mathbf{J} . x_{S+} and x_{S-} refer respectively to points placed just above and just under the line source. The rest of the problem's resolution depends exclusively on the boundary conditions. These latter are the same as in Section 3.1. Thus, expressions of the magnetic field \mathbf{H} excited by \mathbf{J} are obtained by replacing, in expressions of \mathbf{H} excited by \mathbf{M} (see Section 3.1), the term " $\omega \varepsilon \mathbf{M}$ " by the term " $(k_z J_x - k_x J_z) \cdot \mathbf{e}_y$ ".

It is worth noting that, at any point, the electric field \mathbf{E} is deduced from the magnetic field \mathbf{H} .

4. HYBRIDIZATION METHOD

In this part, we present the hybrid expansion method we have developed. We first explain the general principle. Next, we deal with the choice of the optimum GB's waist and the limits of the two expansion domains. We then present the way we calculate expansion coefficients. In Section 4.4, we introduce the test case to assess our method. Finally we present our hybrid expansion method's performances and propose a default parameter setting giving good results for general cases.

4.1. Method Principle

Figure 5 presents an antenna radiating a TM field \mathbf{H}_{rad} in media 1 and 2. We suppose that this antenna excites Surface Waves (SW) and/or Leaky Waves (LW) on the interface between media 1 and 2 [11,12]. We assume that the initial field \mathbf{H}^i on the expansion surface S_{exp} is known. We want to expand \mathbf{H}^i in terms of Gaussian Beams (GB). However, near the interface, the field due to SW and LW strongly interacts with the interface. We cannot model this interaction with GB. Thus, in this area, we expand \mathbf{H}^i in Surface Equivalent Currents (SEC) instead. Figure 5 presents the two resulting expansion domains. In our method we start by defining the limits of these two expansion domains (Section 4.2). Then we calculate the expansion coefficients for GBs (red) and SECs (blue dots) (Section 4.3). Finally we compute the recombined field at any point M by adding the contributions of both the expansion GBs and the expansion SECs.

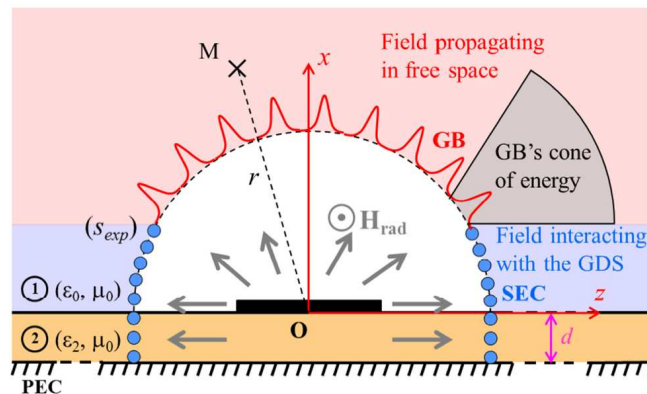


Figure 5. Field expansion, around an antenna, using both Surface Equivalent Currents (blue dots) and Gaussian Beams (red lines).

4.2. Expansion Domains Limits

The method used in order to choose the limits between the two expansion domains is the same on both sides of Ox axis. In the present case, we therefore limit our study to the area corresponding to $z > 0$. The initial field \mathbf{H}^i is expanded on S_{exp} in term of N GBs of center O_n (n running from 1 to N) and M SECs placed at Q_m (m running from 1 to M), as shown on Figure 6(a). In first approach we choose to set $Q_1 = O_N$. We will discuss later the benefit of freeing this constraint.

The choice of the expansion domain limits results from the following constraint: no elementary GB must interact with the Grounded Dielectric Slab (GDS). Actually this constraint applies only to GB_N , the last GB. Hence, we have to determine, on the one hand, O_N the center of GB_N located on the expansion surface S_{exp} and, on the other hand, W_0 the waist of the elementary GBs. The problem comes down to simple geometrical considerations, when assuming S_{exp} circular with a radius r_{exp} greater than the far field distance of the antenna. By this way, O_N is expressed by its cylindrical coordinates $(r_{\text{exp}}, \theta_N)$, and \mathbf{P}_N , the Poynting's vector of the initial field at O_N , can be assumed normal to S_{exp} (Figure 6(b)).

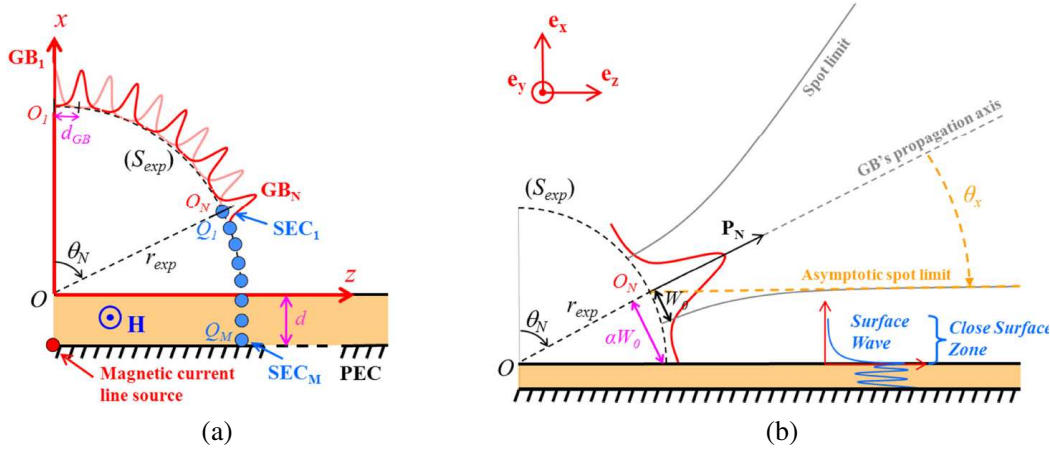


Figure 6. (a) Field expansion, around a current-line excited interface, using both SECs and GBs; (b) zoom on the positioning of O_N , last GB center, according to $\alpha \cdot W_0$, θ_N , r_{exp} and θ_x .

The above-mentioned constraint leads O_N and W_0 to satisfy two criteria:

- At S_{exp} level, the amplitude of GB_N must be minimal on the GDS (Figure 6(b)). This amplitude can be adjusted by the parameter α (see Section 2.1). We will discuss later how the expansion accuracy depends on this parameter. This criterion is written as follows:

$$\tan \theta_N = \frac{r_{\text{exp}}}{\alpha W_0} \quad (5)$$

- The far field of GB_N must not illuminate the GDS. As \mathbf{P}_N is oriented according to θ_N , the asymptotic spot limit of GB_N is oriented according to $\theta_N + \theta_x$. We remind that θ_x is the divergence angle of the elementary GBs. Finally, as the GDS matches an angle of $\pi/2$, θ_N satisfies the following requirement:

$$\theta_N = \frac{\pi}{2} - \theta_x \quad (6)$$

which leads to

$$\tan \theta_N = 1 / \tan \theta_x \quad (7)$$

In order to satisfy the paraxial approximation, we need $\theta_x < 20^\circ$, leading to $\tan(\theta_x) \approx \theta_x$. Introducing this simplification and (1) in Equation (5), and applying to (7), we find:

$$W_0^2 = \frac{2 \cdot r_{\text{exp}}}{\alpha \cdot k} \quad (8)$$

From (8), we can derive O_n coordinates. We observe that W_0 and O_N depend on r_{exp} , radius of S_{exp} , and the parameter α . The main impact of the latter on the method will be studied in detail in Section 4.5. In order to assess the influence of r_{exp} , we set in the following figures $\alpha = 1.5$ which stands for a suitable value.

On Figure 7(a), we plot W_0 as a function of r_{exp} . As expected, W_0 grows with r_{exp} . However this growth is not homothetic according to r_{exp} : W_0/λ_0 grows only from 1.1 to 2.1 when r_{exp}/λ_0 grows from 5 to 20. From W_0 we can deduce the number of expansion GBs used, which is plotted on Figure 7(b). This number increases with r_{exp} due to the not homothetic growth of W_0 according to r_{exp} . This leads the proportion of expansion surface covered by expansion GBs to increase with r_{exp} . We show on Figure 7(c) this fill rate which represents the surface covered by expansion GBs compared to the whole surface of expansion S_{exp} . In fact the maximization of this fill rate is one of our objectives as it leads to favor GB expansion over SEC expansion.

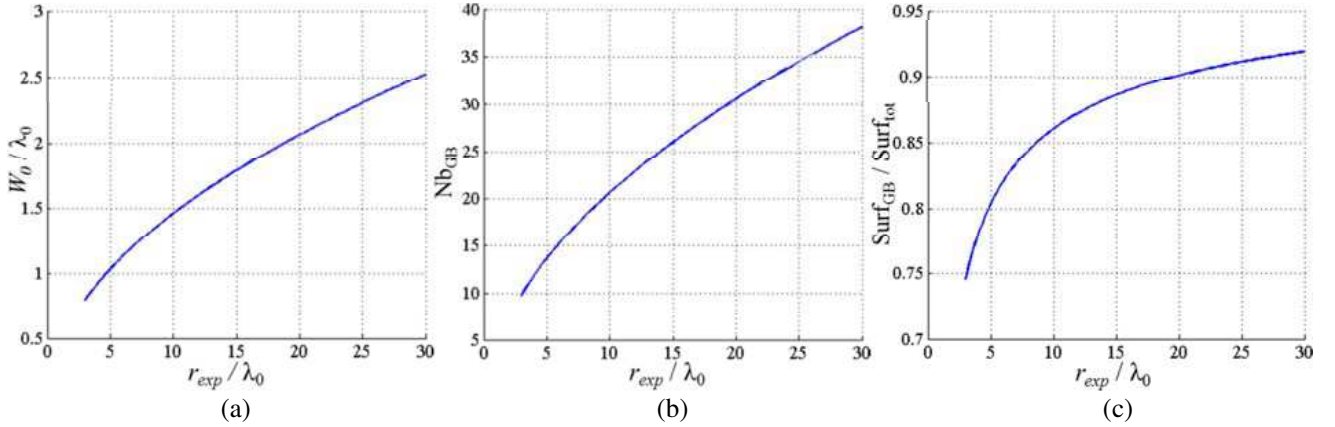


Figure 7. (a) W_0 ; (b) number of expansion GBs; (c) proportion of S_{exp} covered by the GB expansion, as a function of r_{exp} , for $\alpha = 1.5$ and $d_{GB} = 0.9 \cdot W_0$.

4.3. Expansion Coefficients Calculation

Expansion limits chosen in Section 4.2, leads to the position of O_N and the value of W_0 (Figure 6(b)). We then deduce the position of points O_n , where the GB expansion will be carried out. The mesh step d_{GB} is chosen equal to $0.9 \cdot W_0$ as defined in [7]. We also deduce the positions of points Q_m , where the SEC expansion will be carried out. Here we choose a classical mesh step of $\lambda/8$, with λ the free space wave length in the considered medium.

We start by expanding in N GBs the initial field on points O_n . We then have to expand the rest of the field in M SECs. However, this latest step requires some precautions. Indeed, the abrupt truncation of the GB expansion leads to an error on the SEC expansion. On Q_m points, the magnetic and electric field error caused by GB expansion can be written respectively:

$$\begin{aligned} \mathbf{H}_{\text{ErrGB}}(Q_m) &= \sum_{n=1}^N \mathbf{H}_{\text{GB}_n}(Q_m) \\ \mathbf{E}_{\text{ErrGB}}(Q_m) &= \sum_{n=1}^N \mathbf{E}_{\text{GB}_n}(Q_m) \end{aligned} \quad (9)$$

This error involves a wrong radiated field which can be canceled by subtracting $\mathbf{H}_{\text{ErrGB}}$ and $\mathbf{E}_{\text{ErrGB}}$ to the initial field on each point Q_m . When applying this correction, the electric and magnetic elementary currents, \mathbf{J} and \mathbf{M} respectively, corresponding to the SEC expansion, are defined as follows:

$$\begin{aligned} \mathbf{J}(Q_m) &= \mathbf{n} \times \left(\mathbf{H}^i(Q_m) - \sum_{n=1}^N \mathbf{H}_{\text{GB}_n}(Q_m) \right) \\ \mathbf{M}(Q_m) &= -\mathbf{n} \times \left(\mathbf{E}^i(Q_m) - \sum_{n=1}^N \mathbf{E}_{\text{GB}_n}(Q_m) \right) \end{aligned} \quad (10)$$

\mathbf{n} being the unity vector normal to S_{exp} at Q_m .

4.4. Test Configuration

For convenience, we choose to use as reference, a field calculated by our SEC radiating code. This field results from the excitation of a GDS by a SEC and must be representative of any radiated field. The GDS is chosen in order to obtain a radiated field \mathbf{H}_{rad} combination of a free space radiation and a SW radiation (Figure 8(a)). The free space radiation is given by 2 Leaky Waves radiating at 45° and 80° . The SW radiation is given by 6 surface modes. This behavior is obtained at 10 GHz for a slab of height $d = 6$ cm [20]. The excitation is a magnetic current line source (red point) oriented and infinite along \mathbf{e}_y and placed at $x = -d$ as in [13]. Medium 1 is air and the structure is infinite along \mathbf{e}_z and invariant along the y direction. With this excitation, only TM modes (with the magnetic field oriented along \mathbf{e}_y) can propagate and the resulting field is symmetric according to \mathbf{e}_x axis [13]. Figure 8(a) shows a cartography, in the xOz plane, of the field radiated by this structure. Maximums of radiation are not for $\theta = 0$ as they correspond to LW radiation. The SW field presents some ripples along the interface. This is due to positive and destructive interactions between all 6 surface modes which do not have the same phase speeds along \mathbf{e}_z [13, 20]. Figure 8(b) shows a radiation pattern at $r = 40 \cdot \lambda_0$. We can notice that the maximum far field is caused by the SW at 90° .

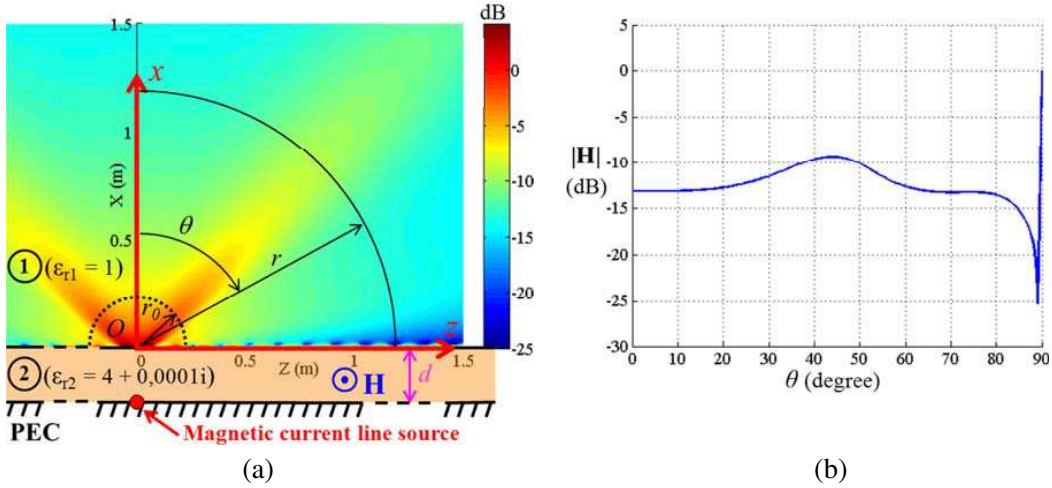


Figure 8. (a) Test configuration and radiated field in the xOz plane; (b) radiation pattern at $r = 40 \cdot \lambda_0$ (plain circle in Figure (a)); the field's amplitude is normalized by the maximum of $|\mathbf{H}_{\text{rad}}|$ on the circle $r = r_0$, which defines the expansion surface used in Section 4.5.

Here the far field distance r_0 is approximately obtained from the half power beamwidth ($\theta_{HP} = 32.5^\circ$ according to Figure 8(b)) and confirmed by the circular shape of the front phase of the radiated field. By this means we find $r_0 \approx 7 \cdot \lambda_0 = 21$ cm.

4.5. Hybrid Expansion Method Performances and Parameter Setting

Here we present the performances of our hybrid expansion method as a function of r_{exp} , α and r_{obs} (observation distance).

In order to evaluate the recombination error on the observation points, we define two error criteria computed on S_{obs} , a circular surface of radius r_{obs} :

$$\sigma_{\text{all}} = \frac{\sum_{s_{\text{obs}}} \|\mathbf{H}_{\text{rad}} - \mathbf{H}_{\text{rec}}\|^2}{\sum_{s_{\text{obs}}} \|\mathbf{H}_{\text{rad}}\|^2}, \quad \sigma_{\text{CSZ}} = \frac{\sum_{s_{\text{obsCSZ}}} \|\mathbf{H}_{\text{rad}} - \mathbf{H}_{\text{rec}}\|^2}{\sum_{s_{\text{obsCSZ}}} \|\mathbf{H}_{\text{rad}}\|^2} \quad (11)$$

with \mathbf{H}_{rad} being the reference field, and \mathbf{H}_{rec} being the recombined field. σ_{all} characterizes the recombination error on S_{obs} . σ_{CSZ} characterizes the recombination error on the portion of S_{obs} close to the interface (i.e., containing 99% of the SWs energy, see Figure 6(b)). In our study we consider results good enough when σ is below -30 dB.

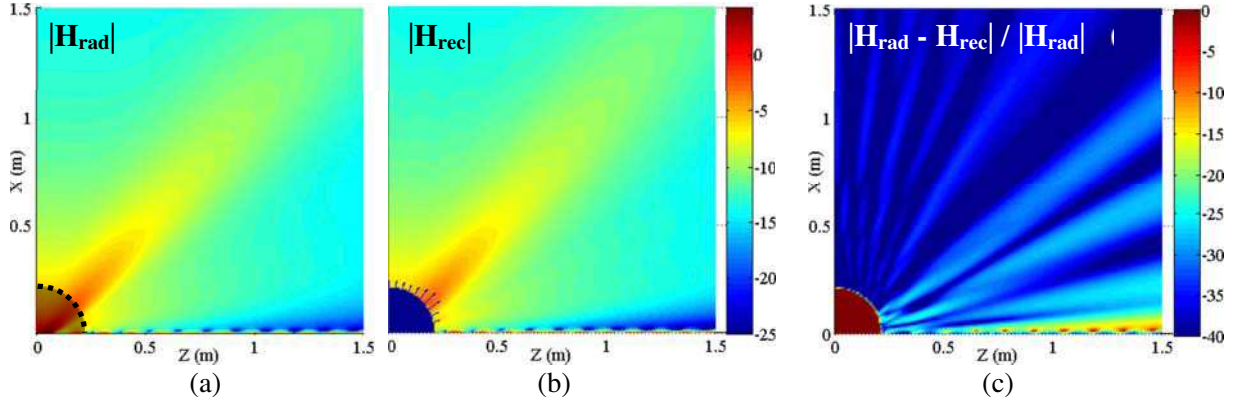


Figure 9. Amplitude (in dB) of (a) reference field and (b) recombined field, normalized by $\max(|\mathbf{H}^i|)$, the maximum field amplitude on the expansion surface; (c) recombination relative error. $r_{\text{exp}} = r_0 = 7 \cdot \lambda_0$, $\alpha = 1.5$ and $d_{GB} = 0.9 \cdot W_0$.

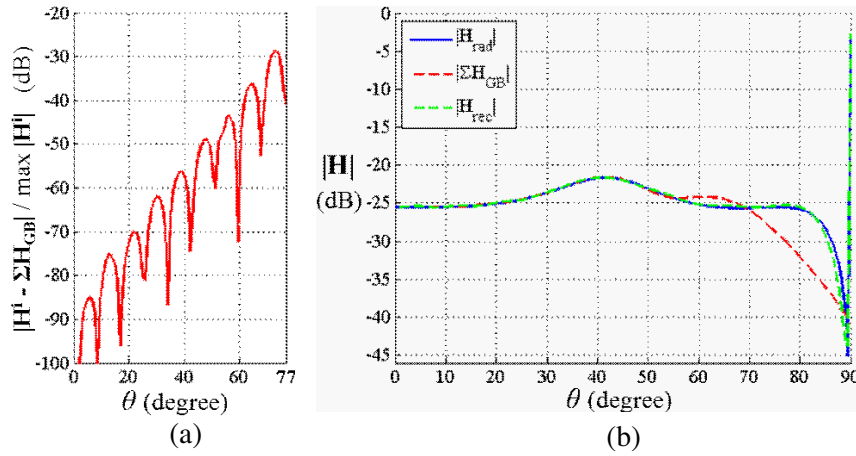


Figure 10. (a) Expansion error in GB; (b) initial and recombined fields at $r_{\text{obs}} = 100 \cdot r_0$. Amplitude normalization by $\max(|\mathbf{H}^i|)$. $r_{\text{exp}} = r_0$, $\alpha = 1.5$ and $d_{GB} = 0.9 \cdot W_0$.

We first study the case where $r_{\text{exp}} = r_0 = 7 \cdot \lambda_0$ (see Section 4.4), $\alpha = 1.5$ and $d_{GB} = 0.9 \cdot W_0$. With this set of parameters $W_0 = 1.14 \cdot \lambda$ and so θ_N , the angle of the last GB center, values 77° . The expanding surface S_{exp} is the dashed circle drawn in Figure 8(a) and Figure 9(a). Figures 9(a) and 9(b) show the amplitude of initial and recombined fields respectively, in the xOz plane. We can see that the recombined field well matches the initial field. The recombination relative error plotted in Figure 9(c) corroborates this observation. This relative error is normalized by $|\mathbf{H}_{\text{rad}}|$ at each point. Thus large errors obtained at angles near $\theta = 89^\circ$ are not of significant importance as they are related to very low values of $|\mathbf{H}_{\text{rad}}|$. On Figure 9(b) are drawn the real Poynting vectors of the expansion GBs (blue arrows). In this case 19 GBs are needed for the GB expansion on S_{exp} .

Figure 10(a) shows the GB expansion error (red line). This expansion error is only considered for angles $\theta < \theta_N = 77^\circ$ on S_{exp} . In fact, for angles $\theta \geq \theta_N$ on S_{exp} , all errors linked to expansion GBs are cancelled by the SEC expansion (see Section 4.3). Here the GB expansion error gives the error criteria $\sigma_{\text{all}}(r_{\text{exp}}) = -36.1$ dB. Figure 10(b) presents results at very far distance ($r_{\text{obs}} = 100 \cdot r_0$): the reference field (blue), the recombined field using only GBs (red) and the recombined field using both GBs and SECs radiation (green). We observe that the recombined field using only expanded GBs radiation gives acceptable errors for angles between 0 and 50° . In contrast, the recombine field using both GBs and SECs radiation give acceptable errors for all angles θ on S_{obs} . The corresponding error criteria is $\sigma_{\text{all}}(100 \cdot r_0) = -30.5$ dB.

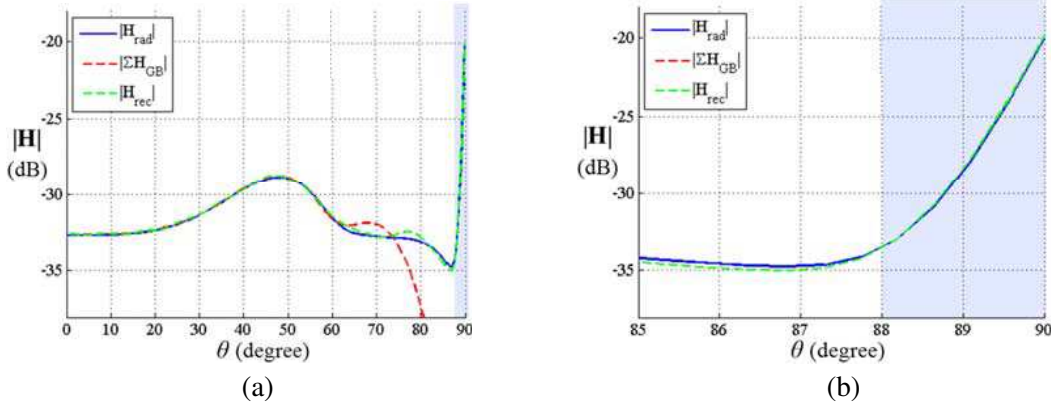


Figure 11. (a) Initial and recombined fields at $r_{obs} = 2 \cdot r_0$; (b) zoom for grazing angles. Amplitude normalization by $\max(|\mathbf{H}^i|)$. $r_{exp} = r_0$, $\alpha = 1.5$ and $d_{GB} = 0.9 \cdot W_0$.

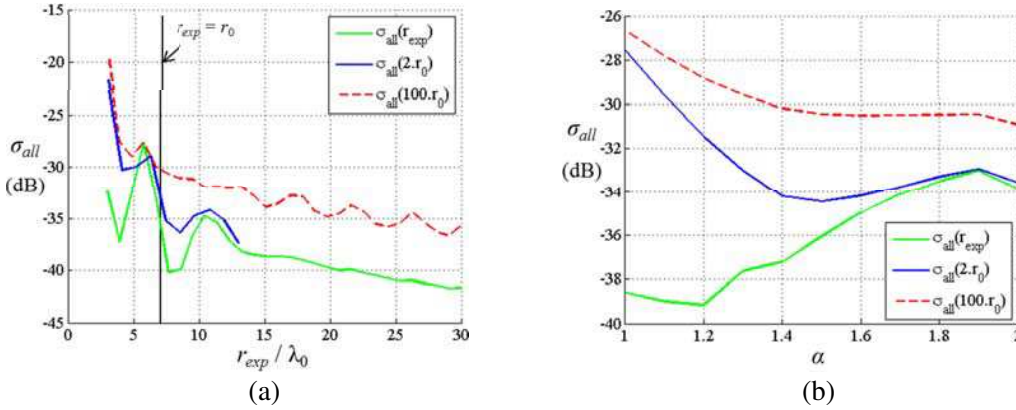


Figure 12. σ_{all} as a function (a) of r_{exp} (for $\alpha = 1.5$) or (b) of α (for $r_{exp} = r_0$). $r_{obs} = r_{exp}$, $2 \cdot r_0$ or $100 \cdot r_0$ and $d_{GB} = 0.9 \cdot W_0$.

Figure 11(a) presents results near from S_{exp} ($r_{obs} = 2 \cdot r_0$). The Close Surface Zone (CSZ) is highlighted in light blue and magnified in Figure 11(b). Here this zone is of height λ_0 . The recombined field using only expanded GBs radiation gives acceptable errors for angles between 0 and 60° . When using both GBs and SECs radiation acceptable errors are obtained for all angles θ on S_{obs} . The corresponding error criteria is $\sigma_{all}(2 \cdot r_0) = -34.2$ dB. Close to the surface we observe that the SW is well approximated, leading to an error $\sigma_{CSZ}(2 \cdot r_0) = -32.4$ dB. In this area one also notes that the field due to expansion GBs is very weak.

The results presented above were obtained for $r_{exp} = r_0$, $\alpha = 1.5$ and $d_{GB} = 0.9 \cdot W_0$. We are now going to study the influence of parameters r_{exp} and α .

On Figure 12(a), we set $\alpha = 1.5$ and plot the evolution of the error criteria σ_{all} as a function of r_{exp} , the expansion surface radius, for the three observation distances used previously: $r_{obs} = r_{exp}$ (green), $2 \cdot r_0$ (blue) and $100 \cdot r_0$ (dashed red). We do not plot σ_{CSZ} , as it always shows acceptable errors (i.e., $\sigma_{CSZ} < -30$ dB). We see that the recombining errors decrease with increasing r_{exp} . When $r_{exp} \geq r_0$ all errors are acceptable (i.e., less than -30 dB). Hence for Figure 12(b), we set $r_{exp} = r_0$ which stands for the worst acceptable case. In Figure 12(b), we show the influence of α on the recombining error for the 3 same observation distances. It is worth noting that we seek to favor the GB expansion over the SEC one. According to Equation (8) this leads to minimize α . From this figure, we first see that the GB expansion is accurate enough for any α . We also observe that $\sigma_{all}(2 \cdot r_0)$ and $\sigma_{all}(100 \cdot r_0)$ tend to decrease when α increases. In fact, for large values of α , the amplitude of the GB_N on the GDS is weak at the expansion surface's level. This leads to less expansion errors, particularly on the expansion of SW and LW. For $\alpha = 1.5$ all recombining errors are acceptable. The setting $\alpha = 1.5$ then stands for

a good compromise.

Precedent results show that good performances can be obtained for $r_{\text{exp}} = r_0$, $\alpha = 1.5$ and $d_{GB} = 0.9 \cdot W_0$. Moreover, applying this parameter setting to other structures also gives good results.

5. DISCUSSION

Precedent results show that good performances can be obtained for $r_{\text{exp}} = r_0$, $\alpha = 1.5$ and $d_{GB} = 0.9 \cdot W_0$. Therefore we can consider that it is a good default parameter setting. Moreover, finer settings enable us to further improve results:

1. We saw that further increasing r_{exp} leads both to favor the GB expansion over the SEC one (Section 4.2) and to better recombining accuracy (Section 4.5). However increasing r_{exp} leads to an increase of the mesh volume needed to compute the electromagnetic field on S_{exp} , which is not suitable. Therefore, the choice of r_{exp} results from a compromise.
2. The GB waist W_0 obtained from (8) is often overestimated. In fact, due to the radiation of LW out of the surface [13], the angle $(\mathbf{e}_x, \mathbf{P}_N)$ is smaller than θ_N . For better results we can modify (8) to take into account the real orientation on the Poynting vector \mathbf{P}_N .
3. In this study, we set $d_{GB} = 0.9 \cdot W_0$. However using $d_{GB} < 0.9 \cdot W_0$ improves the quality of the GB expansion thus leading to better overall results.
4. As a first approach we used $Q_1 = O_N$ in this study. By extending the area of the SEC expansion (i.e., angle $(\mathbf{e}_x, \mathbf{OQ}_1)$ becomes smaller than θ_N) a part of the GB expansion error will be cancelled by the SEC expansion. This will lead to less recombining errors. However this solution gives rise to a lot more SECs to compute, which expands the computing time.

6. CONCLUSION

In this paper, we proposed a method for extending the conventional Gaussian Beam (GB) expansion in order to take into account surface wave and leaky wave excitation and propagation on Grounded Dielectric Slab (GDS), by hybridizing both the GB and the Surface Equivalent Current (SEC) expansions. To do so, we first extended the theory presented in [13, 14] in order to apply, in TM, the SEC theorem to a GDS structure. Then, using geometric criteria, we obtained a closed form formula to determine W_0 , the waist of the expansion GBs. We subsequently deduced directly the limits of the two expansion domains. We showed that increasing the expansion surface radius leads to favor GB expansion over SEC expansion. Good performances were obtained for our hybrid expansion method when applied to a representative radiated field, composed of both free space radiation and surface wave radiation. We found a generic set of parameters which gives good results for all tested cases. Finally we discussed the influence of additional parameters enabling further performance improvements.

Interestingly, this work can easily be transposed to more complex configurations such as multilayer and metamaterial structures [17, 18]. Furthermore, as the GDS is never infinite, the SW diffraction by the truncated GDS must also be taken into account [21]. Finally, we can also consider the extension of this method to 3D cases and to curved surfaces.

ACKNOWLEDGMENT

This work has been funded by both the CNES and Onera — the French Aerospace Lab.

REFERENCES

1. Maciel, J. J. and L. B. Felsen, "Gaussian beam analysis of propagation from an extended plane aperture distribution through dielectric layers. I. Plane layer and II. Circular cylindrical layer," *IEEE Transactions on Antennas and Propagation*, Vol. 38, No. 10, 1607–1617, Oct. 1990.
2. Pascal, O., F. Lemaître, and G. Soum, "Dielectric lens analysis using vectorial multimodal Gaussian beam expansion," *Ann. Telecom.*, Vol. 52, Nos. 9–10, 519–528, 1997.

3. Chou, H. T., P. A. Pathak, and R. J. Burkholder, "Novel Gaussian beam method for the rapid analysis of large reflector antennas," *IEEE Transactions on Antennas and Propagation*, Vol. 49, No. 6, 880–893, 2001.
4. Galdi, V., L. B. Felsen, and D. A. Castanon, "Quasi-ray Gaussian beam algorithm for time-harmonic two-dimensional scattering by moderately rough interfaces," *IEEE Transactions on Antennas and Propagation*, Vol. 49, No. 9, 1305–1314, 2001.
5. Maciel, J. J. and L. B. Felsen, "Gabor-based narrow-waisted Gaussian beam algorithm for transmission of aperture-excited 3D vector fields through arbitrarily shaped 3D dielectric layers," *Radio Science*, Vol. 37, No. 2, vic6.1–6.9, 2002.
6. Ghannoum, I., C. Letrou, and G. Beauquet, "Gaussian beam shooting algorithm based on iterative frame decomposition," *2010 Proceedings of the Fourth European Conference on Antennas and Propagation (EuCAP)*, 1–4, Apr. 12–16, 2010.
7. Chabory, A., J. Sokoloff, S. Bolioli, and P. F. Combes, "Computation of electromagnetic scattering by multilayer dielectric objects using Gaussian beam based techniques," *C. R. Phys.*, No. 6, 654–662, 2005.
8. Chabory, A., J. Sokoloff, and S. Bolioli, "Physics-based expansion on 3D conformal gaussian beams for the scattering from a curved interface," *Progress In Electromagnetics Research B*, Vol. 54, 245–264, 2013.
9. Hillairet, J., J. Sokoloff, and S. Bolioli, "Uniform analytic scattered fields of a PEC plate illuminated by a vector paraxial gaussian beam," *Progress In Electromagnetics Research B*, Vol. 14, 203–217, 2009.
10. Elis, K., A. Chabory, and J. Sokoloff, "3D interaction of Gaussian beams with dichroic surfaces for the modeling of quasi optical systems," *International Symposium on Antenna Technology and Applied Electromagnetics (ANTEM)*, 1–5, Toulouse, France, Jun. 2012.
11. Balanis, C. A., *Modern Antenna Handbook*, John Wiley & Sons, New York, 2008.
12. Capet, N., C. Martel, J. Sokoloff, and O. Pascal, "Optimum high impedance surface configuration for mutual coupling reduction in small antenna arrays," *Progress In Electromagnetics Research B*, Vol. 32, 283–297, 2011.
13. Tamir, T. and A. A. Oliner, "Guided complex waves. Part 1: Fields at an interface; Part 2: Relation to radiation patterns," *Proceedings of the Institution of Electrical Engineers*, Vol. 110, No. 2, 310–334, Feb. 1963.
14. Tamir, T. and L. B. Felsen, "On lateral waves in slab configurations and their relation to other wave types," *IEEE Transactions on Antennas and Propagation*, Vol. 13, No. 3, 410–422, May 1965.
15. Collin, R. E., *Field Theory of Guided Waves*, 2nd Edition, The IEEE Press Series on Electromagnetic Wave Theory, 1991.
16. Balanis, C. A., *Advanced Engineering Electromagnetic*, 2nd Edition, Ch. 7.8, John Wiley & Sons, New York, 2012.
17. Paulus, M., P. Gay-Balmaz, and O. J. F. Martin, "Accurate and efficient computation of the Green's tensor for stratified media," *Phys. Rev. E*, Vol. 14, 5797–5807, 2000.
18. Song, Z., K.-L. Zheng, H.-X. Zhou, J. Hu, and W. Hong, "A method of locating leaky wave poles of spectral Green's functions for a layered medium by consecutive frequency perturbation," *Electrical Design of Advanced Packaging & Systems Symposium*, 1–4, Dec. 2–4, 2009.
19. Kogelnick, H. and T. Li, "Laser beams and resonators," *Proceedings of the IEEE*, Vol. 54, No. 10, 1312–1329, 1966.
20. Hsu, C.-I. G., R. F. Harrington, J. R. Mautz, and T. K. Sarkar, "On the location of leaky wave poles for a grounded dielectric slab," *IEEE Transactions on Microwave Theory and Techniques*, Vol. 39, No. 2, 346–349, Feb. 1991.
21. Chuang, C. W., "Surface wave diffraction by a truncated inhomogeneous dielectric slab recessed in a conducting surface," *IEEE Transactions on Antennas and Propagation*, Vol. 34, No. 4, 496–502, Apr. 1986.